2006

# Kinetics of Microbial Reduction of Solid Phase U(VI)

Chongxuan Liu
*Pacific Northwest National Laboratory*, chongxuan.liu@pnl.gov

Byong-Hun Jeon
*Yonsei University*

John M. Zachara
*Pacific Northwest National Laboratory*, john.zachara@pnl.gov

Zheming Wang
*Pacific Northwest National Laboratory*, Zheming.wang@pnl.gov

Alice Dohnalkova
*Pacific Northwest National Laboratory*

*See next page for additional authors*

*Environ. Sci. Technol.* **2006**, *40,* 6290−6296

# Kinetics of Microbial Reduction of Solid Phase U(VI)

CHONGXUAN LIU,*,† BYONG-HUN JEON,‡ JOHN M. ZACHARA,† ZHEMING WANG,† ALICE DOHNALKOVA,† AND JAMES K. FREDRICKSON†

*Pacific Northwest National Laboratory, Richland, Washington 99352, and Yonsei University, Wonju Kangwon-Do, Korea 220-710*

Sodium boltwoodite ($NaUO_2SiO_3OH{\cdot}1.5\ H_2O$) was used to assess the kinetics of microbial reduction of solid-phase U(VI) by a dissimilatory metal-reducing bacterium (DMRB), *Shewanella oneidensis* strain MR-1. The bioreduction kinetics was studied with Na-boltwoodite in suspension or within alginate beads in a nongrowth medium with lactate as electron donor at pH 6.8 buffered with PIPES. Concentrations of $U(VI)_{tot}$ and cell number were varied to evaluate the coupling of U(VI) dissolution, diffusion, and microbial activity. Microscopic and spectroscopic analyses with transmission electron microscopy (TEM), energy dispersive spectroscopy (EDS), and laser-induced fluorescence spectroscopy (LIFS) collectively indicated that solid-phase U(VI) was first dissolved and diffused out of grain interiors before it was reduced on bacterial surfaces and/or within the periplasm. The kinetics of solid-phase U(VI) bioreduction was well described by a coupled model of bicarbonate-promoted dissolution of Na-boltwoodite, intragrain uranyl diffusion, and Monod type bioreduction kinetics with respect to dissolved U(VI) concentration. The results demonstrated that microbial reduction of solid-phase U(VI) is controlled by coupled biological, chemical, and physical processes.

## Introduction

Biological reduction of U(VI) by dissimilatory metal reducing bacteria (DMRB) and subsequent precipitation of U(IV) has been proposed as a technology to immobilize U(VI) in uranium-contaminated sediments (www.lbl.gov/NABIR). Bioreduction of dissolved U(VI) by DMRB has a half-life ranging from hours in pure cultures (*1*−*3*) to days in sediments with stimulated bacterial activities (*4*, *5*). The rates of bioreduction of U(VI) adsorbed to Fe(III) oxides such as goethite and hematite are comparable to the rates of dissolved U(VI) bioreduction in the absence of sorbing surfaces (*6*, *7*). Limited evidence (*6*, *8*) suggested that sorption can limit U(VI) bioavailability and slow bioreduction rates in sediments. This effect appeared to result from the association of U(VI) with surfaces and solids in micropores or regions in sediments that were not directly accessible to DMRB. A recent study using nitrate (*9*) suggested that microbial reduction of electron acceptors that are associated with sediment micropores could be rate-limited by diffusion. Diffusion could also limit the supply of organic carbon and thus constrain the DMRB reduction of U(VI) in diffusion-controlled zones (*10*).

Microscopic and spectroscopic analysis of uranium-contaminated sediments from the U.S. Department of Energy Hanford site has revealed that uranium often, but not exclusively, exists as uranyl precipitates associated with small fractures and pores within sediment particle grains exhibiting pore sizes of a few micrometers or less (*11*). Various characterization techniques indicated that the precipitates from several important locations were uranyl silicates, most likely in the form of sodium boltwoodite (*11*−*14*), that formed within intragrain fractures of granitic lithic fragments. The intragrain U(VI) precipitates dissolved in under-saturated solutions with a half-life ranging from 1 week to more than 5 months to reach solubility equilibrium, depending on solution chemistry and intragrain U(VI) dissolution and diffusion properties (*14*). Calculations with a coupled model of Na-boltwoodite dissolution and ion diffusion indicated that diffusion significantly decreased the rates of intragrain uranyl mineral dissolution due to diffusion-induced local solubility limitation (*15*). These investigations have revealed a complex coupling of U(VI) geochemical and physical processes in the sediments. The influence of this complex coupling on the kinetics of microbial reduction of U(VI) has not been studied.

Here we report an investigation of the kinetics of microbial reduction of Na-boltwoodite ($NaUO_2SiO_3OH{\cdot}1.5\ H_2O$) by a representative DMRB (*Shewanella oneidensis* strain MR-1). The Na-boltwoodite was used to represent solid-phase U(VI) that may exist within granitic lithic fragments at Hanford. The solid phase was used in suspension and in porous alginate beads to evaluate the influence of intragrain diffusion on the kinetics of microbial reduction. Batch experiments were performed in a nongrowth medium with lactate as electron donor at pH 6.8 buffered with PIPES. Uranium speciation and distribution in the solid phase was monitored by laser-induced fluorescence spectroscopy. The biogenic U(IV) precipitates and their bacterial association were examined by transmission electron microscopy. The insights derived from the microscopic and spectroscopic analyses were used to establish a coupled model of dissolution, intragrain diffusion, and microbial reduction processes. The developed model was then applied to describe the experimental kinetic data of microbial reduction of solid-phase U(VI).

## Experimental Section

**Na-Boltwoodite.** The synthesis and characterization of Na-boltwoodite was described elsewhere (*16*). The synthetic Na-boltwoodite has a solubility (log $K_{sp}$) of 5.85 and a surface area of 30. 8 $m^2/g$.

**Na-Boltwoodite-Entrapped Alginate Beads.** Synthetic Na-boltwoodite powder was entrapped in microporous alginate beads following a procedure described in ref *17*. Alginate (MP Biomedicals, Aurora, OH) was mixed with Na-boltwoodite in DDI water with a final concentration of 6.7 g/L alginate and desired concentrations of Na-boltwoodite. The resulting mixture was dispensed with a syringe and needle (18 gauge) into a cold (4 °C) and degassed 100 mmol/L $CaCl_2$ solution where spherical beads (ca. 2.9 mm in diameter) formed. The beads were matured for 5 min and immediately used in microbial reduction experiments after washing with DDI water to remove excess $CaCl_2$.

* Corresponding author phone: (509) 376-0129; fax: (509) 376-3650; e-mail: Chongxuan.liu@pnl.gov.
† Pacific Northwest National Laboratory.
‡ Yonsei University.


10.1021/es0608601 CCC: $33.50

Published on Web 09/16/2006

**Microorganism and Culture Conditions.** Bacterium *S. oneidensis* strain MR-1 (*18*) was used as a representative DMRB. Strain MR-1 was cultured with tryptic soy broth (TSB), 27.5 g/L (Difco Laboratories, Detroit, MI), harvested by centrifugation, and washed twice with Na-PIPES (Na-1,4-piperazine-*N*,*N*′-bis-2-ethanesulfonic acid) buffer (10 mmol/L, pH 6.8). Cell density was determined by measuring the absorbance at 600 nm. The washed cells were re-suspended in PIPES buffer and purged with $O_2$-free $N_2$ for microbial reduction experiments.

**Bioreduction of U(VI).** Microbial reduction experiments were conducted using 125 mL glass serum bottles in an anaerobic chamber (Coy Laboratory Products, Inc.) filled with 97% Ar and 3% $H_2$. Anoxic solutions of Na-PIPES (10 mmol/L), Na-lactate (10 mmol/L), and $CaCl_2$ (5 mmol/L) were added to reactors followed by the addition of either Na-boltwoodite powder or Na-boltwoodite-entrapped alginate beads (ca. 360 beads, 5 mL) to provide final U(VI) concentrations of 0.6 or 4.4 mmol/L. The reactors were capped with thick butyl rubber stoppers and crimp sealed. Sodium bicarbonate (10 mmol/L) was added with a syringe and needle, and the solution pH was adjusted to 6.8 with 0.1 mol/L HCl or NaOH. Calcium was added to maintain the stability of alginate beads in suspensions. It is a chemical component in Hanford porewaters with a concentration range of 0.5 to 50 mmol/L and a median of about 5 mmol/L (*19*). MR-1 cells were injected in the reactors when Na-boltwoodite dissolved close to a steady state. The suspensions were gently shaken on an orbital shaker at room temperature.

**Analytical Techniques.** At select times, 0.5 mL of solution was withdrawn from each reactor, filtered (0.2 $\mu$m), and acidified (0.01 mol/L $HNO_3$ final concentration) in the anaerobic chamber, and then analyzed for dissolved U(VI) with a Kinetic Phosphorescence Analyzer (KPA; Chemcheck Instruments, Richland, WA). The total solution volume withdrawn from each bottle was less than 10 mL (<10% of total solution volume) during the entire experiment. Solution pH was measured using an Orion 250A+ pH meter with a combination pH/temperature probe.

**Laser-Induced Fluorescence Spectroscopy (LIFS).** LIFS measurements were performed in a Cryo Industries RC-152 cryostat near liquid He-temperature (5.5 ± 1.0 K) as described previously (*20*). U(VI)-containing alginate beads were sampled at select times from the reactors. The bead samples were frozen with liquid nitrogen and each bead was cut into halves with a blade in the anaerobic chamber. One half was directly mounted in a custom-built sealed copper sample holder. The other half was removed from the anaerobic chamber, mounted on the sample holder, and oxidized by reacting with 10% $H_2O_2$. Time-resolved emission spectra were recorded using a thermoelectrically cooled Princeton Instruments PIMAX time-gated intensified CCD camera that was triggered by the delayed output of the laser pulse ($\lambda_{ex}$ = 415 nm) and controlled by the WinSpec data acquisition software. Data were analyzed using IGOR, a commercial software, and the Globals program (*21*).

**Transmission Electron Microscopy (TEM).** At selected times, samples for high-resolution TEM were prepared in an anaerobic glovebox. Cells were washed 3 times with anoxic 0.1 mol/L Na cacodyalate buffer at pH 7.2 followed by 3 washes with anoxic deionized water. The cells were pelleted, fixed in glutaraldehyde, dehydrated in series of EtOH, and embedded in LR White resin. The polymerized blocks were anaerobically sectioned on a microtome, and thin sections were mounted on copper grids coated with Formvar and carbon. The prepared samples were removed from glovebox and examined on a JEOL 2010 TEM with an acceleration voltage of 200 kV. The elemental composition of cell-associated precipitates was determined using energy dispersive spectroscopy (EDS) (Oxford Instruments).

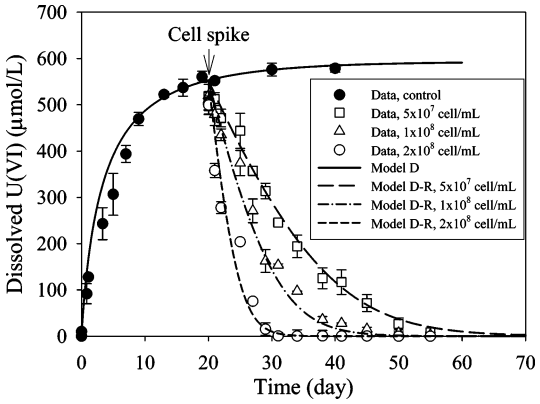


**FIGURE 1. Dissolution of Na-boltwoodite and microbial reduction of U(VI). Symbols and lines are experimental and model results, respectively. Model *D* couples dissolution kinetics (eq 1) with aqueous speciation reaction in Table 2, and model *D*−*R* couples model *D* with microbial reduction of aqueous U(VI) (Table 1). Initial Na-boltwoodite = 0.6 mmol/L.**

## Results and Discussion

**Dissolution.** The dissolution of Na-boltwoodite (Figure 1) was well described by the following rate expression:

$$\frac{d[\mathrm{U(VI)}]_{aq}}{dt} = kA\rho_b \frac{[\mathrm{HCO_3^-}]}{K_{bc} + [\mathrm{HCO_3^-}]} [1 - (\mathrm{IAP}/K_{sp})^n] \qquad (1)$$

where symbol definitions and parameter values are given in Table 1. Calculations were performed with the computer program Geochemist Workbench 6.0 (*22*), by coupling Na-boltwoodite dissolution (eq 1) and equilibrium speciation reactions (Table 2). The rate expression of Na-boltwoodite dissolution (eq 1) was characterized elsewhere (*15*) in bicarbonate solutions that were dominated by either species $UO_2(CO_3)_2^{2-}$ or $UO_2(CO_3)_3^{4-}$. This previously calibrated rate expression well-described the dissolution data in Figure 1 even though the dominant aqueous U(VI) species in the current study was $Ca_2UO_2(CO_3)_3$. The excellent agreement between the dissolution model (*D*) and the data indicated that the effect of aqueous uranyl speciation on Na-boltwoodite dissolution was adequately considered through the thermodynamic affinity term (i.e., IAP/$K_{sp}$) in eq 1.

**Microbial Reduction.** The addition of MR-1 in solutions that had experienced 20 days of Na-boltwoodite dissolution led to an immediate decrease in aqueous U(VI) concentrations (Figure 1). The decrease of aqueous U(VI) concentrations was faster in solutions with higher cell concentrations, indicating the expected consequence of increasing cell concentration on bioreduction rate. The aqueous uranyl concentration fell below detection (<$10^{-9}$ mol/L) after 10−35 days of microbial reduction depending on initial cell concentration. Yellow U(VI) solids were visually absent in all the reactors when aqueous U(VI) concentration decreased to zero, indicating that all the Na-boltwoodite (0.6 mmol/L) was dissolved and microbially reduced at the end of the experiments.

The dissolution and microbial reduction could be effectively described by coupling the dissolution kinetics (eq 1), equilibrium speciation reactions (Table 2), and a non-growth Monod-type rate with respect to aqueous U(VI) concentration

$$\frac{d[\mathrm{U(VI)}]_{aq}}{dt} = -\frac{V_m[\mathrm{U(VI)}]_{aq}}{K_s + [\mathrm{U(VI)}]_{aq}} X \qquad (2)$$

where symbols and parameter values are defined in Table 1. Equation 2 was previously used to describe the microbial

**TABLE 1. Processes, Models, and Parameters for Microbial Reduction of Na-boltwoodite**

**(1) Dissolution of Na-boltwoodite**

$$Na[UO_2(Si_3OH)](H_2O)_{1.5} + 3\,H^+ = UO_2^{2+} + Na^+ + H_4SiO_4 + 1.5H_2O \qquad \log K_{sp} = 5.85$$

$$R = \frac{d[U(VI)]_{aq}}{dt} = kA\rho_b \frac{[HCO_3^-]}{K_{bc} + [HCO_3^-]}[1 - (IAP/K_{sp})^n]$$

$k$, rate constant ($2.05 \times 10^{-6}$ mol/m$^2$/h); $A$, Na-boltwoodite surface area (30.8 m$^2$/g); $\rho_b$, Na-boltwoodite concentration (g/L); $K_{bc}$, half-rate constant with respect to bicarbonate ($2.74 \times 10^{-3}$ mol/L);, IAP and $K_{sp}$, ion activity product and solubility constant (5.85) for Na-boltwoodite, respectively; $n$, reaction order of nonlinearity (0.2); $[HCO_3^-]$, bicarbonate concentration (mol/L).

**(2) Reduction of dissolved U(VI) by DMRB in nongrowth media**

$$Lactate^- + 2UO_2^{2+} + 2H_2O = Acetate^- + 2UO_2(s) + HCO_3^- + 5H^+ \qquad \log K = 21.49$$

$$R = \frac{d[U(VI)]_{aq}}{dt} = -\frac{V_m[U(VI)]_{aq}}{K_s + [U(VI)]_{aq}}X$$

$V_m$, maximum rate ($4.23 \times 10^{-17}$ mol/cell/h); $K_s$, half-rate constant with respect to total aqueous U(VI) ($3.7 \times 10^{-4}$ mol/L); $[U(VI)]_{aq}$, total aqueous U(VI) concentration (mol/L); and $X$, cell concentration (cell/L).

**(3) Diffusion of dissolved U(VI) in spheres**

$$\frac{\partial C}{\partial t} = \frac{\partial}{r^2 \partial r}\left(r^2 D_{eff}\frac{\partial C}{\partial r}\right)$$

$D_{eff}$, effective diffusion coefficient ($2.19 \times 10^{-11}$ m$^2$/s).

**TABLE 2. Equilibrium Speciation Reactions Used in Modeling**

| speciation reaction | log $K$ ($I = 0$) | ref |
|---|---|---|
| $UO_2^{2+} + H_2O = UO_2\,OH^+ + H^+$ | −5.25 | 29 |
| $UO_2^{2+} + 2H_2O = UO_2\,(OH)_2(aq) + 2H^+$ | −12.15 | 29 |
| $UO_2^{2+} + 3H_2O = UO_2\,(OH)_3^- + 3H^+$ | −20.25 | 29 |
| $UO_2^{2+} + 4H_2O = UO_2\,(OH)_4^{2-} + 4H^+$ | −32.40 | 29 |
| $2UO_2^{2+} + H_2O = (UO_2)_2\,OH^{3+} + H^+$ | −2.70 | 29 |
| $2UO_2^{2+} + 2H_2O = (UO_2)_2\,(OH)_2^{2+} + 2H^+$ | −5.62 | 29 |
| $3UO_2^{2+} + 4H_2O = (UO_2)_3\,(OH)_4^{2+} + 4H^+$ | −11.90 | 29 |
| $3UO_2^{2+} + 5H_2O = (UO_2)_3\,(OH)_5^{+} + 5H^+$ | −15.55 | 29 |
| $3UO_2^{2+} + 7H_2O = (UO_2)_3\,(OH)_7^{-} + 7H^+$ | −32.20 | 29 |
| $4UO_2^{2+} + 7H_2O = (UO_2)_4\,(OH)_7^{+} + 7H^+$ | −21.90 | 29 |
| $UO_2^{2+} + CO_3^{2-} = UO_2CO_3(aq)$ | 9.94 | 29 |
| $UO_2^{2+} + 2CO_3^{2-} = UO_2(CO_3)_2^{2-}$ | 16.61 | 29 |
| $UO_2^{2+} + 3CO_3^{2-} = UO_2(CO_3)_3^{4-}$ | 21.84 | 29 |
| $3UO_2^{2+} + 6CO_3^{2-} = (UO_2)_3(CO_3)_6^{6-}$ | 54.00 | 29 |
| $2UO_2^{2+} + CO_3^{2-} + 3H_2O = (UO_2)_2CO_3(OH)_3^- + 3H^+$ | −0.86 | 29 |
| $3UO_2^{2+} + CO_3^{2-} + 3H_2O = (UO_2)_3O(OH)_2HCO_3^+ + 3H^+$ | 0.65 | 29 |
| $2Ca^{2+} + UO_2^{2+} + 3CO_3^{2-} = Ca_2UO_2(CO_3)_3$ | 29.80 | 30 |
| $UO_2^{2+} + Cl^- = UO_2Cl^+$ | 0.17 | 29 |
| $UO_2^{2+} + 2Cl^- = UO_2Cl_2(aq)$ | −1.10 | 29 |
| $UO_2^{2+} + H_4SiO_4 = UO_2H_3SiO_4^+ + H^+$ | −1.84 | 29 |
| $CO_2(g) + H_2O = H_2CO_3$ | −1.47 | 29 |
| $H_2CO_3 = H^+ + HCO_3^-$ | −6.35 | 29 |
| $H_2CO_3 = 2H^+ + CO_3^{2-}$ | −16.68 | 29 |
| $H_4SiO_4 = H^+ + H_3SiO_4^-$ | −23.14 | 29 |
| $H_4SiO_4 = 2H^+ + H_2SiO_4^{2-}$ | −9.84 | 29 |
| $Ca^{2+} + CO_3^{2-} = CaCO_3(aq)$ | 2.48 | 31 |
| $Ca^{2+} + CO_3^{2-} + H^+ = CaHCO_3^+$ | 11.43 | 31 |

reduction of aqueous U(VI) by various DMRB including *S. alga* strain BrY (*23*), *S. putrefaciens* strain CN32 (*2*), and *Geobacter sulfurreducens* (*24*), and a sulfate reducing bacteria *Desulfovibrio desulfuricans* (ATCC7757) (*1*). The rate constants in eq 2 were estimated to be $V_m = 1.1 \times 10^{-15}$ mol/cell/h and $K_s = 3.7 \times 10^{-4}$ mol/L for CN32 (*2*) and these values were comparable to those reported for other DMRB (*3*, *23*, *24*).

The calculations resulting from the coupling of eqs 1 and 2, and speciation reactions (Table 2), however, indicated that the literature maximum rate $V_m$ ($1.1 \times 10^{-15}$ mol/cell/h) that was estimated from CN32 was too large to describe the bioreduction behavior of *S. oneidensis* strain MR-1. Consequently we adjusted $V_m$ by trial-and-error to fit the measured aqueous U(VI) concentrations as a function of time and cell concentration in Figure 1. The best fitted value of $V_m$ was $4.23 \times 10^{-17}$ mol/cell/h, which was about 2 orders of magnitude lower than the previously reported values. The coupled dissolution−reduction ($D$−$R$) model with the new $V_m$ for eq 2 well-described the decrease of aqueous U(VI) concentration as a function of time and cell concentration (Figure 1). The lower new value for $V_m$ was attributed to the dominant presence of aqueous uranyl species $Ca_2UO_2(CO_3)_3$. A recent study showed that species $Ca_2UO_2(CO_3)_3$ decreased both the rate and extent of U(VI) bioreduction by DMRB (*25*). The literature $V_m$ was determined in solutions containing no calcium. The results in Figure 1 showed that MR-1 could completely reduce aqueous U(VI) in solutions dominated by $Ca_2UO_2(CO_3)_3$, but with a slower kinetic rate than in solutions without $Ca^{2+}$. One study reported that $V_m$ in solutions without $Ca^{2+}$ was $2.0 \times 10^{-15}$ mol/cell/h for Mr-1 (*3*). The result that the same $K_s$ value ($3.7 \times 10^{-4}$ mol/L) was able to describe DMRB reduction of U(VI) in solutions with/without Ca suggested that uranyl affinity with the cells or active enzymatic locations was unaffected by the aqueous speciation differences.

**Microbial Reduction of Entrapped Na-Boltwoodite.** Uranyl dissolution and release to the aqueous phase from Na-boltwoodite (0.6 mmol/L) entrapped in the alginate beads was slightly slower than that from Na-boltwoodite alone (Figure 2), showing the effects of intragrain diffusion. The dotted line in Figure 2 was the calculated aqueous uranyl concentration based on the dissolution model only (i.e., eq 1 coupled with speciation reactions in Table 2). About 85% of entrapped U(VI) was dissolved over 20 days. Biological reduction after the cell spike at 20 days decreased aqueous U(VI) concentrations (Figure 2). The aqueous U(VI) concentrations decreased at a similar rate as in Figure 1 for both cell numbers over the first 10 days of contact. After this period, aqueous U(VI) concentrations in the reactor with $2 \times 10^8$ cell/mL were close to, but above, the detection limit for an additional 30 days. In the reactor with $1 \times 10^8$ cell/mL, the aqueous U(VI) concentration decreased at a much slower rate after 15 days than it did in the Na-boltwoodite suspension, indicating that microbial reduction was slower at late stage in the presence of entrapped U(VI).

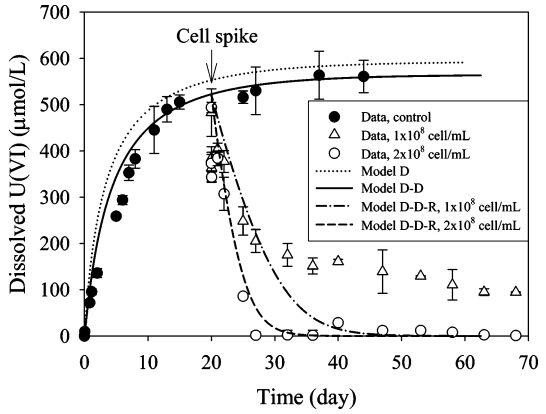


**FIGURE 2. Dissolution and release of U(VI) from entrapped Na-boltwoodite and microbial reduction of dissolved U(VI). Symbols and lines are experimental and model results, respectively. Model *D* is described in Figure 1 caption. Model *D*−*D* couples model *D* with effective intragrain uranyl diffusion (eqs 3−6); Model *D*−*D*−*R* couples model *D*−*D* with microbial reduction of aqueous U(VI) (eq 2). Initial Na-boltwoodite = 0.6 mmol/L.**

Visual observations showed that yellowish 0.6 mmol/L, Na-boltwoodite-entrapped beads gradually became clear with increasing time during the microbial reduction phase, indicating U(VI) depletion from the beads. LIFS analysis, however, indicated that residual Na-boltwoodite was present in the bead samples collected at 30 days of bioreduction (or 50 days from experiment start) in both 0.6 mmol/L U(VI) reactors (Figure 3). Time-resolved LIFS analysis of the beads displayed a spectral signature consistent with Na-boltwoodite (Figure 3a), while LIFS imaging showed increasing U(VI) intensity (white) toward the bead center (Figure 3b). These measurements revealed that Na-boltwoodite was partially dissolved and that diffusive release progressed from the bead edges toward the interiors as expected. At short lifetime (<1 $\mu$s), there were background increases in the two short wavelength peaks (510 and 530 nm), suggesting minor transformation of Na-boltwoodite with incubation. This minor component was likely the uranyl ion that partially replaced calcium in bridging alginate molecules. Independent experiments by mixing uranyl nitrate with alginate confirmed that uranyl ions, like calcium, can aggregate alginates. Identical time-resolved LIFS spectra and similar U(VI) distribution were observed from bead samples treated with $H_2O_2$, suggesting that U(IV) was not associated with intragrain regions.

Measurements with the Acridine Orange Direct Count (AODC) method indicated that total cell concentrations decreased by 7 and 13% at 7 days, and 36 and 26% at 30 days in the reactors with $1 \times 10^8$ and $2 \times 10^8$ cell/mL, respectively. The partial loss in cell concentration with time may have caused the decreased microbial reduction rates at late stage. TEM analysis revealed that U(IV) precipitated as extracellular aggregates and in association with cell surfaces including a significant mass within the cell periplasm (Figure 4). The accumulated uranium precipitates on cell surfaces and in periplasms increased with increasing time. Some of the cells were highly encrusted with $UO_{2(s)}$. U precipitation may have interfered with cell structural integrity or metabolism. TEM images showed that cell walls became compromised with time, with some cells producing vesicle-like features while others lysed. Such accumulation of $UO_{2(s)}$ and extracellular production of vesicle-like materials has also been observed in a recent study of microbial reduction of aqueous U(VI) (uranyl acetate) in 30 mmol/L bicarbonate solution (*26*). The decrease of microbial reduction rate at late stage may be attributed to (i) decreased aqueous U(VI) concentration as indicated in eq 2, and (ii) an overall decrease in cell viability and respiration rate. Such "respiration stress" occurred in the presence of entrapped Na-boltwoodite, and not when the U(VI) phase was freely suspended in solution. The mechanism for this phenomenon was unclear.

To further study the coupling of dissolution, diffusion, and microbial reduction, another set of experiments was performed with a higher initial entrapped U(VI) concentration (4.4 mmol/L). The rate of U(VI) dissolution and release to the aqueous phase nearly doubled in the reactors with 4.4 mmol/L initial Na-boltwoodite concentration (Figure 5) as compared to those with 0.6 mmol/L (Figure 2), because dissolution kinetics were proportional to Na-boltwoodite surface area (eq 1). Higher entrapped U(VI) concentrations also drove greater uranyl diffusive fluxes to the aqueous phase. After 10 days of dissolution/diffusion, the aqueous U(VI) concentration was close to solubility equilibrium (Figure 5). Unlike in Figures 1 and 2 where most Na-boltwoodite was dissolved (about 85−90%) before cell spiking, here most U(VI) (84%) still remained as entrapped Na-boltwoodite at the dissolution steady-state. The addition of MR-1 led to the decrease of aqueous U(VI) concentration in all reactors (Figure 5). The rate of aqueous U(VI) concentration decrease was slower than that shown in Figure 2 at comparable cell concentrations because of the faster and continuous supply of aqueous U(VI) from the dissolution of entrapped Na-boltwoodite.

The rapid decrease in aqueous U(VI) concentration followed MR-1 addition (Figure 5) indicated that U(VI) supply from intragrain dissolution/diffusion was slower than the rate of microbial reduction. The microbial reduction of aqueous U(VI) caused the undersaturation of the bulk solution with respect to Na-boltwoodite and thus increased the rates of dissolution/diffusion (eq 1). On the other hand, the decrease of aqueous U(VI) concentration slowed microbial reduction rate according to eq 2. The integrated effect of these processes was to slow the decrease of aqueous U(VI) concentration after its initial fast rate phase (Figure 5). Aqueous U(VI) concentrations in solutions with higher cell concentrations were always lower in both fast and slow rate phases because microbial reduction rate increased with higher cell concentrations (eq 2). These results displayed the coupled effects of dissolution/diffusion and microbial activities on the observed aqueous U(VI) concentrations.

After 20 days of microbial reduction, aqueous U(VI) concentrations approached steady state in the reactors with initial cell concentrations of $4 \times 10^8$ and $5 \times 10^8$ cell/L (Figure 5). These results were similar to Figure 2 and were attributed to an overall decrease in cell respiration rate beyond that observed with Na-boltwoodite alone.

**Modeling Coupled Dissolution, Diffusion, and Microbial Reduction.** TEM analysis indicated that U(IV) accumulated on cell surfaces and/or within the periplasm, the presumed locations for enzymatic reduction (*26*). LIFS analysis indicated that intragrain U(VI) distribution was not affected by the oxidation treatment (10% $H_2O_2$) of alginate beads, suggesting no U(IV) association with the beads. The TEM and LIFS analyses collectively indicated that U(VI) dissolved and diffused out of intragrain regions before it was microbially reduced.

Uranyl diffusion in the intragrain regions may be described by a spherical diffusion model

$$\frac{\partial C}{\partial t} = \frac{\partial}{r^2 \partial r}\left(D_{\text{eff}} r^2 \frac{\partial C}{\partial r}\right) + R_1 \qquad (3)$$

where $C$ is the aqueous concentration in alginate beads, $D_{eff}$ is the effective diffusivity of U(VI) within the beads, and $R_1$ is the dissolution rate described by eq 1. The boundary conditions were assumed as follows:

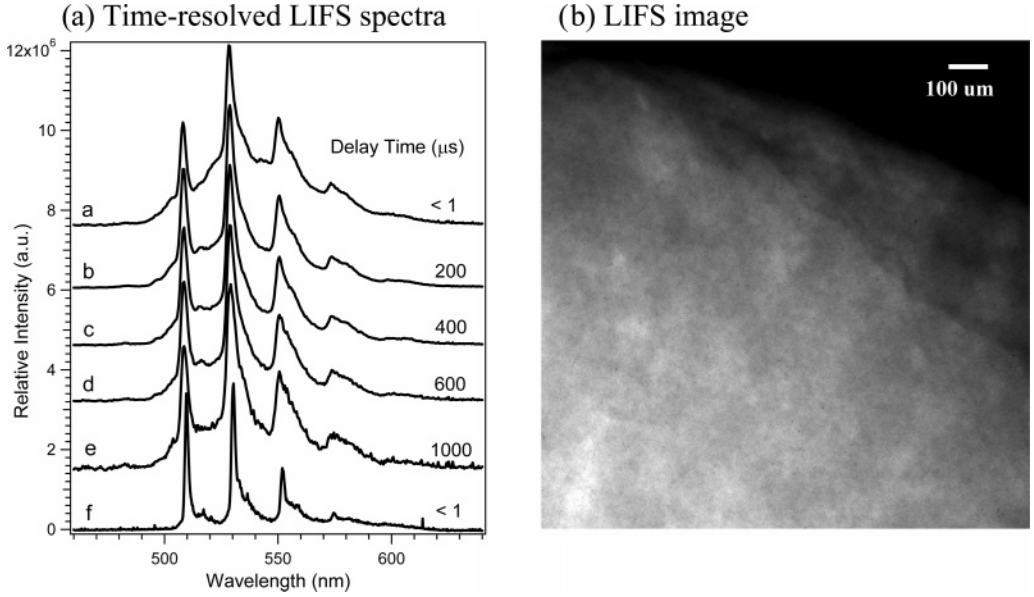


**FIGURE 3. LIFS analysis showing (a) time-resolved spectra of Na-boltwoodite at liquid helium temperature and the distribution of entrapped U(VI) intensity (white) (b). In (a), curve f is for Na-boltwoodite before dissolution and microbial reduction; other curves are for the residual Na-boltwoodite within alginate beads after dissolution and microbial reduction.**

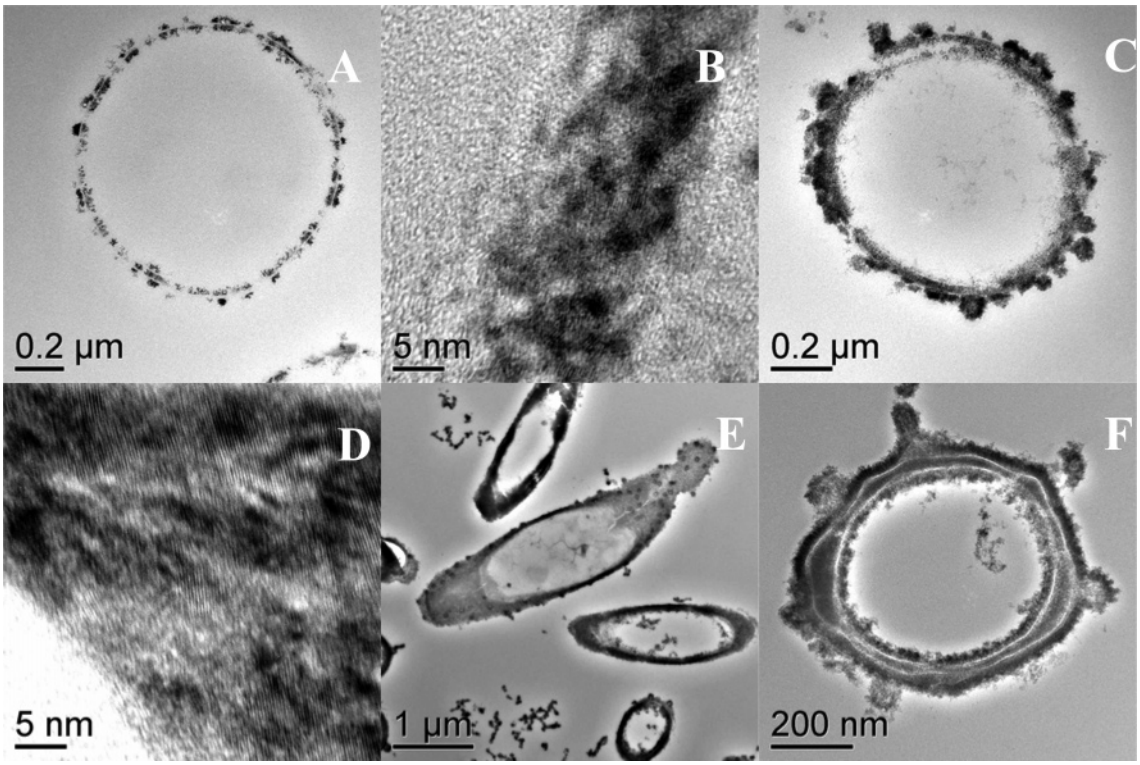


**FIGURE 4. TEM images showing $UO_2$ accumulation on cell surfaces and in periplasms. Samples for images A (a sectioned cell) and B (part of a cell periplasm) were collected at 2 days, samples for images C (a sectioned cell) and D (part of a cell periplasm) were collected at 7 days, and samples for images E and F were collected at 100 days after cell spike.**

$$\left.\frac{\partial C}{\partial r}\right|_{r=0} = 0 \tag{4}$$

$$C|_{r=d/2} = C_b \tag{5}$$

where $d$ is the bead diameter (2.9 mm); and $C_b$ is the aqueous uranyl concentration in the bulk solution, which was governed by the following mass balance equation:

$$\frac{dC_b}{dt} = -\frac{4\pi N D_{eff}}{V} r^2 \left.\frac{\partial C}{\partial r}\right|_{r=d/2} + R_2 \tag{6}$$

where $N$ is the total number (360) of beads in each solution, $V$ is the volume of solution, and $R_2$ is the microbial reduction rate (eq 2). Note that the diffusion of the uranyl ion is affected by the diffusion of other ions due to ion pairing and complexation and their charge coupling. The involved ions, ion pairs, and complexes may each exhibit different diffusivities. A rigorous reactive ion diffusion model can be established to describe uranyl diffusion that includes complexation and speciation coupling (*15*), but that approach was not taken here. Such models are complex and involve

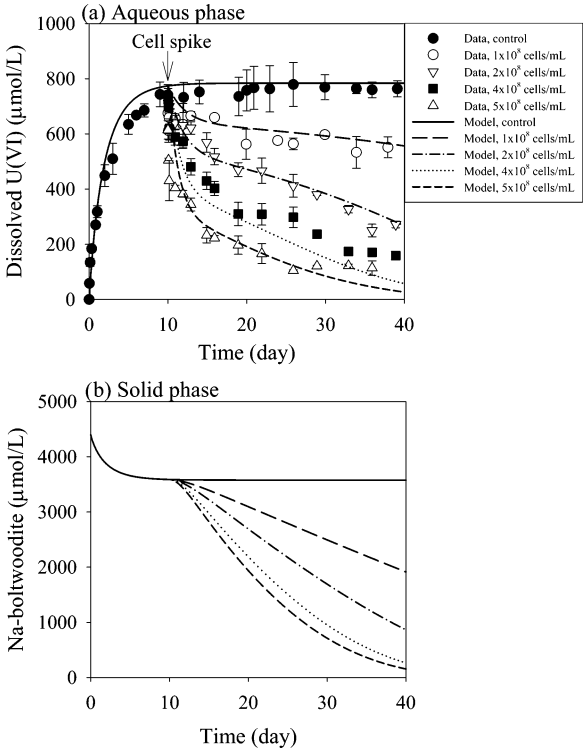


**FIGURE 5. Experimental and modeling results of U(VI) release from entrapped Na-boltwoodite and microbial reduction of dissolved U(VI). Models are described in Figure 2 caption and Table 1. Initial Na-boltwoodite = 4.4 mmol/L.**

many parameters (e.g., diffusivity values for all aqueous species) that are difficult to determine.

Here we assumed that uranyl diffusion from the alginate beads could be effectively described by eqs 3−6 with an effective diffusivity, $D_{eff}$. The effective diffusivity was determined by fitting the experimental data of dissolution/diffusion in Figure 2 using the coupled model of eqs 1, 3−6, and speciation reactions in Table 2. Note that $R_2$ (microbial reduction rate) for this dissolution/diffusion step was zero. The best fitted $D_{eff}$ was $2.19 \times 10^{-11}$ m$^2$/s with the calculated aqueous U(VI) concentration (D−D model line) in Figure 2. The $D_{eff}$ value was 19 times less than the diffusivity for uranyl ion ($UO_2^{2+}$) in water ($4.26 \times 10^{-10}$ m$^2$/s). The slower effective diffusivity indicated that the major uranyl species $Ca_2UO_2(CO_3)_{3aq}$ diffused at slower rates than $UO_2^{2+}$, and/or the pores within alginate beads were tortuous (*27*).

The coupled model of dissolution, diffusion, and microbial reduction (eqs 1−6) with independently determined parameters (Table 1) was then used to calculate the microbial reduction of U(VI) as a function of time with variable cell and Na-boltwoodite concentrations in Figures 2 and 5. The coupled model well predicted the changes of aqueous U(VI) concentrations within 10 days, but under-predicted those after 10 days of bioreduction for the low concentration suspension (0.6 mmol/L; Figure 2). Loss in cell viability or inhibited respiration due to periplasmic U(IV) precipitation was not considered in the model. The model better predicted the microbial reduction of U(VI) with higher initial Na-boltwoodite concentration (4.0 mmol/L, Figure 5), but was unable to predict the apparent steady-state concentrations that evolved in reactors with $4 \times 10^8$ and $5 \times 10^8$ cell/mL over the last three sampling points.

This study demonstrated that the overall rate of DMRB reduction of solid-phase U(VI) required the sequential coupling of dissolution, diffusion (of U(VI) in intragrain), and microbial activities. The apparent diffusivity of U(VI) in the alginate beads ($2.2 \times 10^{-11}$ m$^2$/s) was within the range of U(VI) diffusivity values ($<8.7 \times 10^{-14}$ to $1.7 \times 10^{-10}$ m$^2$/s) in the granitic lithic fragments of the contaminated Hanford sediments (*14*). Two intragrain diffusion domains with distinct diffusivity values were identified in the granitic lithic fragments of the Hanford sediment (*15*). The fast diffusion domain had apparent tortuosity ($D_0/D_a$, where $D_a$ is the apparent intragrain diffusivity, and $D_0$ is the correspondent diffusivity of a species in water) of 1.5 and the slow diffusion domain had a tortuosity of 163. The apparent tortuosity of U(VI) in the alginate beads was 19. It is therefore expected that the overall rate of microbial reduction of Na-boltwoodite in contaminated Hanford sediments with intragrain uranyl-silicate precipitates would be initially rate-limited by microbial rate and activity, and subsequently by diffusion from the slow diffusion domain once uranyl is depleted from the fast diffusion domain.

The accumulation of biogenic U(IV) on cell surfaces or the periplasm could inhibit cell activity and respiration rates. Whether this precipitation-induced rate decrease is applicable to cases where cell growth occurs, and whether intragrain U(VI) in natural sediments could enhance in-situ inhibition are issues that require further study.

The maximum rate ($V_m$ in eq 2) of microbial reduction of uranyl in solutions containing 5 mmol/L Ca was about 2 orders of magnitude slower than the literature values determined in solutions without Ca. Similar findings have been reported in ref *25* which showed that the $Ca_2UO_2(CO_3)_3$ aqueous complex is more resistant to bioreduction than the uranyl carbonate complexes. Hanford groundwater is generally in equilibrium with calcite. The dissolved calcium concentration in equilibrium with calcite and atmospheric $CO_2$(g) at pH 7 was calculated to be 4.7 mmol/L. Spectroscopic analyses indicated that $Ca_2UO_2(CO_3)_3$(aq) is an important species in Hanford pore and ground waters (*20*, *28*). Therefore, it is expected that the rate of microbial reduction of aqueous U(VI) at circumneutral pH in the calcite-containing Hanford sediments would be about two orders of magnitude slower than the rates determined in solutions without calcium.

## Acknowledgments

This research was supported by the U.S. Department of Energy (DOE) through the Environmental Remediation Science Program (ERSP). Pacific Northwest National Laboratory is operated for the DOE by Battelle Memorial Institute under Contract DE-AC05-76RLO1830. A portion of the research described in this paper was performed in the Environmental Molecular Sciences Laboratory, a national scientific user facility sponsored by the Department of Energy's Office of Biological and Environmental Research and located at Pacific Northwest National Laboratory. We thank three reviewers for their constructive comments.

## Literature Cited

(1) Spear, J. R.; Figueroa, L. A.; Honeyman, B. D. Modeling the removal of uranium U(VI) from aqueous solutions in the presence of sulfate reducing bacteria. *Environ. Sci. Technol.* **1999**, *33*, 2667−2675.

(2) Liu, C.; Zachara, J. M.; Fredrickson, J. K.; Kennedy, D. W.; Dohnalkova, A. Modeling the inhibition of the bacterial reduction of U(VI) by $\beta$-$MnO_{2(s)}$. *Environ. Sci. Technol.* **2002**, *36*, 1452−1459.

(3) Liu, C.; Gorby, Y. A.; Zachara, J. M.; Fredrickson, J. K.; Brown, C. F. Reduction Kinetics of Fe(III), Co(III), U(VI), Cr(VI), and Tc(VII) in Cultures of Dissimilatory Metal Reducing Bacteria. *Biotechnol. Bioeng.* **2002**, *80*, 637−649.

(4) Abdelouas, A.; Lu, Y.; Lutze, W.; Nuttall, E. H. Reduction of U(VI) to U(IV) by indigenous bacteria in contaminated ground water. *J. Contam. Hydrol.* **1998**, *35*, 217−233.

(5) Finneran, K. T.; Anderson, R. T.; Nevin, K. P.; Lovley, D. R. Potential for bioremediation of uranium-contaminated aquifers with microbial U(VI) reduction. *Soil Sediment Contam.* **2002**, *11*, 339−357.

(6) Jeon, B.-H.; Kelly, S. D.; Kemner, K. M.; Barnett, M. O.; Burgos, W. D.; Dempsey, B. A.; Roden, E. E. Microbial reduction of U(VI) at the solid−water interface. *Environ. Sci. Technol.* **2004**, *38*, 5649−5655.
(7) Fredrickson, J. K.; Zachara, J. M.; Kennedy, D. W.; Duff, M. C.; Gorby, Y. A.; Li, S.-M.; Krupka, K. M. Reduction of U(VI) in goethite (α-FeOOH) suspensions by a dissimilatory metal-reducing bacterium. *Geochim. Cosmochim. Acta.* **2000**, *64*, 3085−3098.
(8) Ortiz-Bernad, I.; Anderson, R. T.; Vrionis, H. A.; Lovley, D. R. Resistance of solid phase U(VI) to microbial reduction during in situ bioremediation of uranium-contaminated groundwater. *Appl. Environ. Microbiol.* **2004**, *70*, 7558−7560.
(9) Luo, J.; Cirpka, O. A.; Wu, W.; Fienen, M. N.; Jardine, P. M.; Mehlhorn, T. L.; Watson, D. B.; Criddle, C. S.; Kitanidis, P. K. Mass-Transfer Limitation for Nitrate Removal in a Uranium-Contaminated Aquifer. *Environ. Sci. Technol.* **2005**, *39*, 8453−8459.
(10) Tokunaga, T. K.; Wan, J.; Pena, J.; Brodie, E. L.; Firestone, M. K.; Hazen, T. C.; Sutton, S. R.; Lanzirotti, A.; Newville, M. Uranium reduction in sediments under diffusion-limited transport of organic carbon. *Environ. Sci. Technol.* **2005**, *39*, 7077−7083.
(11) McKinley, J. P.; Zachara, J. M.; Liu, C.; Heald, S. M. Microscale Controls on the Fate of Contaminant Uranium in the Vadose Zone, Hanford Site, Washington. *Geochim. Cosmochim. Acta.* **2006**, *70*, 1873−1887.
(12) Catalano, J. G.; Heald, S. M.; Zachara, J. M.; Brown, G. E. J. Spectroscopic and diffraction study of uranium speciation in contaminated vadose zone sediments from the Hanford site, Washington. *Environ. Sci. Technol.* **2004**, *38*, 2822−2828.
(13) Wang, Z.; Zachara, J. M.; Gassman, P. L.; Liu, C.; Qafoku, O.; Catalano, J. G. Fluorescence spectroscopy of U(VI)-silicate and U(VI)-contaminated Hanford sediment. *Geochim. Cosmochim. Acta.* **2005**, *69*, 1391−1403.
(14) Liu, C.; Zachara, J. M.; Qafoku, O.; McKinley, J. P.; Heald, S. M.; Wang, Z. Dissolution of Uranyl Microprecipitates from Subsurface Sediments at Hanford Site, USA. *Geochim. Cosmochim. Acta.* **2004**, *68*, 4519−4537.
(15) Liu, C.; Zachara, J. M.; Yantansee, W.; Majors, P. D.; McKinley, J. P. Microscopic reactive diffusion of uranium in the contaminated sediments at Hanford, USA: Characterization and Modeling. *Water Resour. Res.* **2006**, in press.
(16) Ilton, E. S.; Liu, C.; Yantansee, W.; Wang, Z.; Moore, D.; Zachara, J. M. The effect of carbonate on the dissolution of synthetic Na-boltwoodite. *Geochim. Cosmochim. Acta* **2006**, in press.
(17) Nevin, K. P.; Lovley, D. R. Lack of production of electron-shuttling compounds or solubilization of Fe(III) during reduction of insoluble Fe(III) oxides *Geobacter metallireducens*. *Appl. Environ. Microbiol.* **2000**, *66*, 2248−2251.
(18) Myers, C. R.; Nealson, K. H. Bacterial manganese reduction and growth with manganese oxide as the sole electron acceptor. *Science* **1988**, *240*, 1319−1321.
(19) Serne, R. J.; Lindenmeirer, C. W.; Kutnyakov, I. V.; Last, G. V.; Lindberg, M. J.; Baum, S. R.; Gee, G. W.; Clayton, R. E.; Geiszler, K. N.; Schaef, H. T.; LeGore, V. L.; Brown, C. F.; Lanigan, D. C.; Orr, R. D.; Valenta, M. M.; Hill, T. S. *Characterization of Vadose Zone Sediment: Borehole 299-E33-45 Near Tank B-102 in the B-BX-BY Waste Management Area*; Pacific Northwest National Laboratory: Richland, WA, 2002.
(20) Wang, Z.; Zachara, J. M.; Yantansee, W.; Gassman, P. L.; Liu, C.; Joly, A. G. Cryogenic laser induced fluorescence characterization of U(VI) in Hanford vadose zone pore waters. *Environ. Sci. Technol.* **2004**, *38*, 5591−5597.
(21) Beechem, J. M.; Gratton, E.; Mantulin, W. W. *Globals Unlimited*; UIUC Publication: Urbana, IL, 1991.
(22) Bethke, C. M. *Geochemist Workbench Release 6.0*; University of Illinois: Urbana-Champaign, IL, 2005.
(23) Truex, M. J.; Peyton, B. M.; Valentine, N. B.; Gorby, Y. A. Kinetics of U(VI) reduction by a dissimilatory Fe(III)-reducing bacterium under non-growth conditions. *Biotechnol. Bioeng.* **1997**, *55*, 490−496.
(24) Roden, E. E.; Scheibe, T. D. Conceptual and numerical model of uranium(VI) reductive immobilization in fractured subsurface sediments. *Chemosphere* **2005**, *59*, 617−628.
(25) Brooks, S. C.; Fredrickson, J. K.; Carroll, S.L.; Kennedy, D. W.; Zachara, J. M.; Flymale, A. E.; Kelly, S. D.; Kemner, K. M.; Fendorf, S. Inhibition of bacterial U(VI) reduction by calcium. *Environ. Sci. Technol.* **2003**, *37*, 1850−1858.
(26) Marshall, M. J.; Beliaev, A. S.; Dohnalkova, A. C.; Kennedy, D. W.; Shi, L.; Wang, Z.; Boyanov, M. I.; Lai, B.; Kemner, K. M.; McLean, J. S.; Reed, S. B.; Culley, D. E.; Bailey, V. L.; Simonson, C. J.; Saffarini, D. A.; Romine, M. F.; Gorby, Y. A.; Zachara, J. M.; Fredrickson, J. K. c-Type Cytochrome-Dependent Formation of U(IV) Nanoparticles by Shewanella oneidensis. *PLoS Biol.* **2006**, *4*, 1324−1333.
(27) van Beinum, W.; Beulke, S.; Brown, C. D. Pesticide sorption and diffusion in natural clay loam aggregates. *J. Agric. Food Chem.* **2005**, *53*, 9146−9154.
(28) Dong, W.; Ball, W. P.; Liu, C.; Wang, Z.; Stone, A. T.; Bai, J.; Zachara, J. M. Influence of Calcite and Dissolved Calcium on U(VI) Sorption to a Hanford Subsurface Sediment. *Environ. Sci. Technol.* **2005**, *39*, 7949−7955.
(29) Guillaumount, R.; Fanghänet, T.; Neck, V.; Fuger, J.; Palmer, D. A.; Grenthe, I.; Rand, M. H. *Update on the Chemical Thermodynamics of Uranium, Neptunium, Plutonium, Americium and Technetium*; Elsevier B.V: Amsterdam, The Netherlands, 2003.
(30) Kalmykov, S. N.; Choppin, G. R. Mixed $Ca^{2+}/UO_2^{2+}/CO_3^{2-}$ complex formation at different ionic strengths. *Radiochim. Acta.* **2000**, *88*, 603−606.
(31) NIST. *Critically Selected Stability Constants of Metal Complexes Database, Version 6.0 for Windows*; U.S. Department of Commerce: Gaithersburg, MD, 2001.

*Received for review April 10, 2006. Revised manuscript received August 10, 2006. Accepted August 14, 2006.*

ES0608601